

Multifunctional Theranostic Carbazole-Based Cyanine for Real-Time Imaging of Amyloid- β and Therapeutic Treatment of Multiple Pathologies in Alzheimer's Disease

Chen Chen^{‡ a,b}, Xueli Wang^{‡,b,e}, Di Xu^b, Hailong Zhang^b, Hei-Nga Chan^b, Zhonghao Zhang^a, Shizheng Jia^a, Qingting Song^d, Guoli Song^{a,c,*}, Hung-Wing Li^{d,*} and Man Shing Wong^{b,*}

^aShenzhen Key Laboratory of Marine Bioresources and Ecology, College of Life Sciences and Oceanography, Shenzhen University, Shenzhen, China

E-mail: lilys@szu.edu.cn

^bDepartment of Chemistry, Hong Kong Baptist University, Kowloon Tong, Hong Kong, SAR China

E-mail: mswong@hkbu.edu.hk

^cShenzhen Bay Laboratory, Shenzhen, China.

E-mail: lilys@szu.edu.cn

^dDepartment of Chemistry, Chinese University of Hong Kong, Shatin, Hong Kong, SAR China.

E-mail: hungwingli@cuhk.edu.hk

^ePresent address: College of Pharmaceutical Sciences, Hebei University, Baoding 071002, China

[‡]Chen Chen, Xueli Wang contributed equally.

Table of contents

Experimental Procedures		S5
Scheme S1.	Synthetic Scheme for SLCOOH .	S10
Fig. S1A.	UV-vis absorption and emission spectra of SLCOOH .	S11
Fig. S1B.	Fluorescence spectra of SLCOOH (10 μ M) in the presence of 10 μ M of A β ₁₋₄₂ fibril, Tau-441 aggregate, BSA, α -Synuclein, IgM, IgG, HAS (Human Serum Albumin), L-Gys (L-Cysteine), IAPP (islet amyloid polypeptide) and PrP (prion protein) in 25 mM phosphate buffer (pH = 7.4).	S11
Fig. S1C.	The pH effect on the fluorescence intensity of SLCOOH (30 μ M) in 0.2 M phosphate buffer. Data are expressed as the mean \pm SD of three independent measurements (n = 3).	S12
Fig. S1D.	The time courses of fluorescence intensity of SLCOOH (30 μ M) in the presence and absence of A β ₁₋₄₂ fibrils (150 μ M).	S12
Fig. S1E.	Fluorescence titration of A β ₁₋₄₂ species with SLCOOH and the respective saturation binding curves of SLCOOH to A β ₁₋₄₂ species, respectively.	S13
Fig. S1F.	Plots of fluorescence change of SLCOOH (5 μ M) in the presence of various concentrations of A β ₁₋₄₂ fibril, A β ₁₋₄₂ oligomer and A β ₁₋₄₂ monomer in 25 mM phosphate buffer (pH = 7.4).	S14
Fig. S1G.	Fluorescence displacement assay spectra of ThT /A β ₁₋₄₂ fibril complex (ThT, 5 μ M/A β ₁₋₄₂ fibrils, 10 μ M) by adding SLCOOH (c = 0-10 μ M) stepwise into the complex in 25 mM phosphate buffer (pH = 7.4) obtained by an excitation at 420 nm.	S15
Fig. S1H.	Isothermal titration calorimetry (ITC) binding profiles of SLCOOH and A β ₁₋₄₂ .	S15-16
Table S1.	Summary of optical properties of SLCOOH	S16
Table S2.	Dissociation constant (K_d) value and limit of detection (LOD) of SLCOOH to various A β ₁₋₄₂ species, respectively estimated from the fluorescence titration of A β ₁₋₄₂ species with SLCOOH .	S16

Fig. S2.	Plots of the results of ThT fluorescence assay of A β ₁₋₄₂ in the presence of SLCOOH .	S16
Fig. S3.	Cell viability values (%) estimated by MTT proliferation. Human neuroblastoma SH-SY5Y neuronal cells were treated with different concentrations of SLCOOH at 37 °C for 24 h.	S17
Fig. S4.	Neuroprotective effect of SLCOOH against A β ₁₋₄₂ species toward SH-SY5Y neuronal cells.	S17
Fig. S5.	LC-ESI-MS spectra of brain extracts of the SLCOOH -treated mice.	S18
Fig. S6.	<i>Ex vivo</i> images of SLCOOH in brain slices of (A) 6-month-old 5XFAD Tg and (B) age-matched WT mice co-localized with ThS and a primary antibody (6E10 and 4G8) and then a secondary antibody conjugated with Alexa 488.	S19
Fig. S7.	SLCOOH treatment reduces A β levels in the hippocampus of AD mice. (a) Western blot analysis of A β , APP, and BACE1 protein levels in the hippocampus. (b) Densitometric analysis of (a). (c) Western blot analysis of A β , APP, and BACE1 protein levels in the cortex. (d) Densitometric analysis of (c) ($\#p < 0.05$, $\#\#\#p < 0.01$, $*p < 0.05$, $n = 6$).	S19
Fig. S8.	SLCOOH reduces tau hyperphosphorylation by inhibiting the activity of GSK3 β but not PP2A in vivo. (a, b) Representative Western blot images (a) and quantification (b) of GSK3, <i>p</i> -GSK3 β (Ser9), PP2A, <i>p</i> -PP2A (Tyr307), expression levels in the hippocampus of WT, control mice and SLCOOH -treated. (c, d) Representative Western blot images (c) and (d) of the expression levels of these kinases in the cortex ($\#p < 0.05$, $*p < 0.05$, $n = 6$).	S20
Fig. S9.	SLCOOH promotes the formation of autophagosomes but not ubiquitin proteasomal system. (a, b) Representative Western blot images (a) and quantification (b) of LC3II/LC3I and ubiquitin protein expression levels in the hippocampus of WT, control and SLCOOH -treated mice. (c, d) Representative Western blot images (c) and quantification (d) of the expression levels of these kinases in the cortex ($\#p < 0.05$, $*p < 0.05$, $n = 6$).	S21

Fig. S10.	SLCOOH increases initiation of autophagy pathway in vivo. (a, b) Representative Western blot images (a) and quantification (b) of mTOR/P-mTOR, and p70S6K/P-p70S6K, Beclin 1, p62, cathepsin D expression levels in the hippocampus of WT, control mice and SLCOOH -treated. GAPDH was used as the loading control. (c, d) Representative Western blot images (c) and quantification (d) of the expression levels of these kinases in the cortex. GAPDH was used as the loading control. (# $p < 0.05$, * $p < 0.05$, 1, n = 6).	S22
Fig. S11.	(a) Representative western blots of PSD95 and Synaptophysin in the hippocampus and cortex. GAPDH was used as the loading control. (b and c) Densitometric analyses of the data in (a). (b) Hippocampus. (c) Cortex. (## $p < 0.01$, * $p < 0.05$, ** $p < 0.01$, n = 6).	S23
Fig. S12.	(a) Representative western blots of CaMKII, p-CaMKII, ERK, p-ERK, CREB and p-CREB in the hippocampus and cortex of WT, AD and SLCOOH mice at 6 months. GAPDH was used as the loading control. (b-c) Densitometric analyses of the data in (a) (means \pm SEMs). (b) Hippocampus. (c) Cortex. (# $p < 0.05$, ## $p < 0.01$, * $p < 0.05$, **** $p < 0.0001$. n = 6.).	S23
Fig. S13.	SLCOOH alleviated the overload of intracellular Ca ²⁺ in 3×Tg AD mice primary neurons. (a) Representative confocal images of intracellular Ca ²⁺ in primary AD neurons transfected with AAV9-jRCaMP1. (Scale bar: 20 μ m) (b) The quantification of intracellular Ca ²⁺ level. (** $p < 0.01$, n = 6 cells; The data was quantified from three independent experiments)	S24
Fig. S14.	SLCOOH decreases the intracellular Ca ²⁺ level through downregulating the expression level of NMDAR2B. (a) Representative western blots of NMDAR2A, p-NMDAR2A, NMDAR2B, p-NMDAR2A in the hippocampus and cortex of WT, AD and SLCOOH mice at 6 months. GAPDH was used as the loading control. (b-c) Densitometric analyses of the data in hippocampus (b) and cortex (c). (# $p < 0.05$, * $p < 0.05$, n = 6.).	S25
Fig. S15.	¹ H and ¹³ C NMR and HRMS spectra of SLCOOH .	S26-27
Fig. S16.	A HPLC trace of synthesized SLCOOH .	S27

Experimental:**Synthesis of 9-(2-(2-methoxyethoxy)ethyl)-9H-carbazole, 2**

To a solution of carbazole (3.34 g, 20 mmol) in DMF (80 mL) at 0 °C was added NaH (0.72 g, 30 mmol). After heating at 80 °C for 1.5 h, 1-chloro-2-(2-methoxyethoxy)ethane (3.31g, 24 mmol) was added dropwise. The resulting mixture was kept at 80 °C overnight. After cooling down to 0 °C, the reaction mixture was carefully quenched with water and extracted with ethyl acetate three times. The combined organic phase was washed with water and brine. Then the organic layer was dried over anhydrous sodium sulfate and the solvent was removed. The residue was purified by silica gel chromatography using petroleum ether and ethyl acetate as eluent (EA:PE = 1:3) to afford alkylated carbazole 5 (4.46 g) as brown oil in 83% yield. ¹H NMR (400 MHz, CDCl₃) δ 8.09 (d, *J* = 7.6 Hz, 2H), 7.46 (m, 4H), 7.23 (m, 2H), 4.51 (t, *J* = 6.4 Hz, 2H), 3.86 (t, *J* = 6.4 Hz, 2H), 3.52 (m, 2H), 3.42 (m, 2H), 3.31 (s, 3H). ¹³C NMR (100 MHz, CDCl₃) δ 140.5, 125.6, 122.8, 120.2, 118.9, 108.7, 71.8, 70.7, 69.1, 59.0, 43.0. MS (FAB) *m/z* Calcd for C₁₇H₁₉NO₂ 269.1 Found 269.2 [M]⁺.

3-Bromo-9-(2-(2-methoxyethoxy)ethyl)-9H-carbazole, 3

To a solution of **2** (2 g, 7.4 mmol) in dichloromethane (60 mL) was added NBS (1.3 g, 7.4 mmol) portion-wise in an ice-water bath. After complete addition, the solution

mixture was warmed to room temperature and stirred overnight. The resulting solution was washed with water and brine. The organic phase was dried over anhydrous sodium sulfate and the solvent were removed. The residue was purified by silica gel chromatography using ethyl acetate and petroleum ether (EA: PE = 1: 5) as eluent to afford **3** (1.75 g) in 68% yield as an oil that can turn into solid after standing. ^1H NMR (400 MHz, CDCl_3) δ 8.16 (d, $J = 2.0$ Hz, 1H), 8.01 (d, $J = 8.0$ Hz, 1H), 7.51 (dd, $J = 8.0$ Hz, 2.0 Hz, 1H), 7.44 (m, 2H), 7.34 (d, $J = 8.4$ Hz, 1H), 7.22 (m, 1H), 4.46 (t, $J = 6.0$ Hz, 2H), 3.83 (t, $J = 6.0$ Hz, 2H), 3.48 (m, 2H), 3.39 (m, 2H), 3.28 (s, 3H). ^{13}C NMR (100 MHz, CDCl_3) δ 140.7, 139.2, 128.2, 126.3, 124.5, 122.8, 121.8, 120.4, 119.3, 111.7, 110.4, 109.0, 71.8, 70.7, 69.1, 59.0, 43.2. MS (FAB) m/z Calcd for $\text{C}_{17}\text{H}_{18}\text{BrNO}_2$ 347.0 Found 347.3 $[\text{M}]^+$.

9-(2-(2-Methoxyethoxy)ethyl)-9H-carbazole-3-carbaldehyde, 4

To a solution of **3** (1.5 g, 4.3 mmol) in dried THF (45 mL) was added *n*-BuLi (3.5 mL 5.2 mmol) at -78 °C. The resulting mixture was stirred at -78 °C for 1 h and then added with dried DMF (3 mL). The reaction mixture was allowed warming up to room temperature and stirred overnight before quenching with aqueous ammonia chloride solution. Water was added and extracted with ethyl acetate three times. The combined organic phase was washed with brine and dried over anhydrous sodium sulfate. After removing the solvent, the residue was purified by silica gel chromatography using ethyl acetate and petroleum ether (EA: PE = 1: 2) as eluent to afford **7** (0.76 g) as yellow solid in 60% yield. ^1H NMR (400 MHz, CDCl_3) δ 10.07 (s, 1H), 8.58 (d, $J = 0.8$ Hz,

1H), 8.13 (d, $J = 8.0$ Hz, 1H), 7.98 (dd, $J = 8.8$ Hz, 0.8 Hz, 1H), 7.51 (m, 3H), 7.30 (m, 1H), 4.53 (t, $J = 6.0$ Hz, 2H), 3.87 (t, $J = 6.0$ Hz, 2H), 3.49 (m, 2H), 3.38 (m, 2H), 3.26 (s, 3H). ^{13}C NMR (100 MHz, CDCl_3) δ 191.8, 144.3, 141.1, 128.5, 127.1, 126.6, 123.7, 123.0, 122.9, 120.6, 120.4, 109.4, 109.3, 71.8, 70.8, 69.1, 59.0, 43.4. MS (FAB) m/z Calcd for $\text{C}_{18}\text{H}_{19}\text{NO}_3$ 297.1 Found 297.3 $[\text{M}]^+$.

(E)-9-(2-(2-Methoxyethoxy)ethyl)-3-(2-(quinolin-4-yl)vinyl)-9H-carbazole, 5

To the solution of lepidine (0.8 g, 5.6 mmol) and 9-(2-(2-methoxyethoxy)ethyl)-9H-carbazole-3-carbaldehyde (1.78 g, 6.0 mmol) in DMF (10 mL) in sealed tube, TMSCl (6.4 mL, 50 mmol) was added and the resulting mixture was heated to 100 °C for 24 h. After cooling down to 0 °C, water was added followed by NaHCO_3 aqueous solution to pH 8. The water solution was extracted with dichloromethane three times. The combined organic phase was washed with brine and dried over anhydrous sodium sulfate. After removing the solvent, the residue was purified by silica gel chromatography using dichloromethane and petroleum ether (DCM: PE = 1: 4) as eluent to afford **5** (1.63 g) in 69% yield. ^1H NMR (400 MHz, CDCl_3) δ 8.85 (d, $J = 4.8$ Hz, 1H), 8.27 (s, 1H), 8.25 (d, $J = 7.6$ Hz, 1H), 8.13 (d, $J = 8.4$ Hz, 1H), 8.12 (d, $J = 7.6$ Hz, 1H), 7.78 (d, $J = 16$ Hz, 1H), 7.73 (d, $J = 6.4$ Hz, 1H), 7.70 (t, $J = 7.6$ Hz, 1H), 7.43-7.58 (m, 6H), 7.26 (t, $J = 7.2$ Hz, 1H), 4.46 (t, $J = 6.0$ Hz, 2H), 3.84 (t, $J = 6.0$ Hz, 2H), 3.49 (t, $J = 5.6$ Hz, 2H), 3.41 (t, $J = 5.6$ Hz, 2H), 3.30 (s, 3H). ^{13}C NMR (100 MHz, CDCl_3) δ 150.0, 148.5, 143.3, 140.9, 140.9, 135.9, 129.9, 129.1, 127.8, 126.3, 126.2, 124.9, 123.5, 123.2, 122.7, 120.3, 119.5, 119.4, 116.3, 109.3, 109.1, 71.8, 70.7,

69.1, 58.9, 43.1. HRMS (MALDI-TOF) m/z Calcd for $C_{28}H_{27}N_2O_2$ 423.2083 Found 423.2067 $[M + H]^+$.

(E)-1-(Carboxymethyl)-4-(2-(9-(2-(2-methoxyethoxy)ethyl)-9H-carbazol-3-yl)vinyl)-quinolinium bromide (SLCOOH)

A solution of **5** (0.21 g, 0.5 mmol) and bromoacetic acid (0.28 g, 2.0 mmol) in ethanol was stirred overnight at room temperature. After removing the solvent, the residue was precipitated from methanol and ethyl acetate to afford **SLCOOH** (0.13 g) in 46% yield.

1H NMR (400 MHz, DMSO- d_6) δ 9.27 (d, $J = 6.8$ Hz, 1H), 9.18 (d, $J = 8.0$ Hz, 1H), 8.90 (s, 1H), 8.62 (d, $J = 7.2$ Hz, 1H), 8.60 (d, $J = 6.8$ Hz, 1H), 8.52 (d, $J = 16$ Hz, 1H), 8.42 (d, $J = 16$ Hz, 1H), 8.32 (d, $J = 8.4$ Hz, 1H), 8.26-8.23 (m, 2H), 8.15 (d, $J = 8.8$ Hz, 1H), 8.06 (t, $J = 7.6$ Hz, 1H), 7.79 (d, $J = 8.4$ Hz, 1H), 7.71 (d, $J = 8.0$ Hz, 1H), 7.53 (t, $J = 7.2$ Hz, 1H), 7.32 (t, $J = 7.2$ Hz, 1H), 5.89 (s, 2H), 4.64 (t, $J = 5.2$ Hz, 2H), 3.84 (t, $J = 5.2$ Hz, 2H), 3.49-3.46 (m, 2H), 3.32-3.29 (m, 2H), 3.11 (s, 3H). ^{13}C NMR (100 MHz, DMSO- d_6) δ 167.9, 154.4, 147.9, 146.3, 142.4, 141.0, 138.7, 135.4, 128.9, 127.6, 126.7, 126.5, 126.1, 122.9, 122.2, 122.1, 120.4, 120.0, 119.0, 116.2, 115.1, 110.6, 110.5, 71.3, 69.8, 68.9, 58.1, 42.9. HRMS (MALDI-TOF) m/z Calcd for $C_{30}H_{29}N_2O_4$ 481.2122 Found 481.2156 $[M]^+$.

***In vivo* NIRF imaging of SLCOOH**

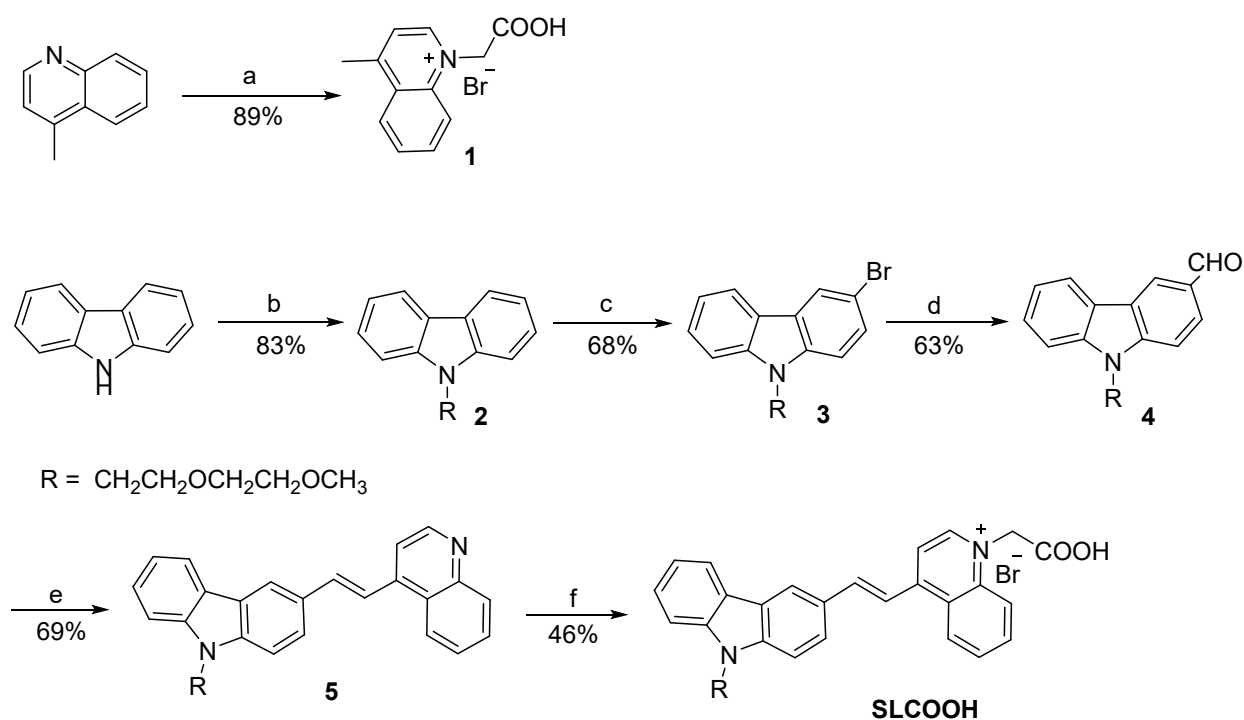
Before background imaging, 5XFAD transgenic mice and age-matched wild-type mice were shaved as controls. Before imaging, oxygen (1.0 mL) was supplemented with isoflurane gas (2.0 mL min^{-1}). The mice were anesthetized under these condition, kept

still, and then injected with 100 μ L of **SLCOOH** (10 mg/kg) through the tail vein. The IVIS imaging system was used to collect fluorescence images from the brain at different time points. A filter set (excitation at 496 nm and emission at 690-700 nm) was used to obtain a fluorescent image with an exposure time of 1 s. Living Image software was used to analyze the image and select the ROI in the brain area. Brain fluorescence intensity was obtained from photon counting. The data were analyzed by normalizing the fluorescence intensity to the background fluorescence of each mouse [i.e. $F(t)/F(\text{pre})$], where $F(t)$ is the fluorescence intensity at the time point of interest and $F(\text{pre})$ is the background fluorescence signal.

Co-staining brain tissues of 5XFAD-Tg mice *ex vivo*

5XFAD transgenic mice were injected with **SLCOOH** *via* tail vein. After 30 minutes, it was deeply anesthetized and perfused intracranially with PBS, and then perfused with 8% formaldehyde in PBS (pH 7.4). After excision, the brain is buried in the optimal cutting temperature compound (OCT), and then the slice is frozen with a cryostat (thickness 10 μ m). Next, 0.4% Triton X-100 was used to infiltrate the free-floating portion and block in a blocking solution containing 2% BSA. For staining by Thio-S, the sections were incubated with 1.0 μ M Thio-S solution for 5-8 minutes, then washed with 25% ethanol for 4 minutes, then washed with PBS for 5 minutes, and then washed in water for 5 minutes. For co-staining studies, free-floating sections were further incubated with primary antibodies, namely 4G8, 6E10 (1:200) at 4°C overnight. Collect the primary antibody the next day. The sections were washed in PBS and incubated in

a 2% BSA solution containing goat anti-mouse or goat anti-rabbit secondary antibodies conjugated with Alexa Fluor 488 (1:500) at room temperature for 2 h. A confocal laser scanning microscope (Leica TCS SP8) at the School of Traditional Chinese Medicine, Hong Kong Baptist University was used to sequentially capture images of A β immunofluorescence reactivity, followed by images of **SLCOOH** on A β species.



Reagents and Conditions: a, BrCH_2COOH , EA, r.t.; b, $\text{ClCH}_2\text{CH}_2\text{OCH}_2\text{CH}_2\text{OCH}_3$, NaH, DMF, 80 °C; c, NBS, DCM, 0 °C to r.t.; d, *n*-BuLi, DMF, THF, -78 °C to r.t.; e, TMSCl, DMF, 100 °C, sealed tube; f, BrCH_2COOH , CH_3CN , r.t.

Scheme S1. Synthetic Scheme for **SLCOOH**.

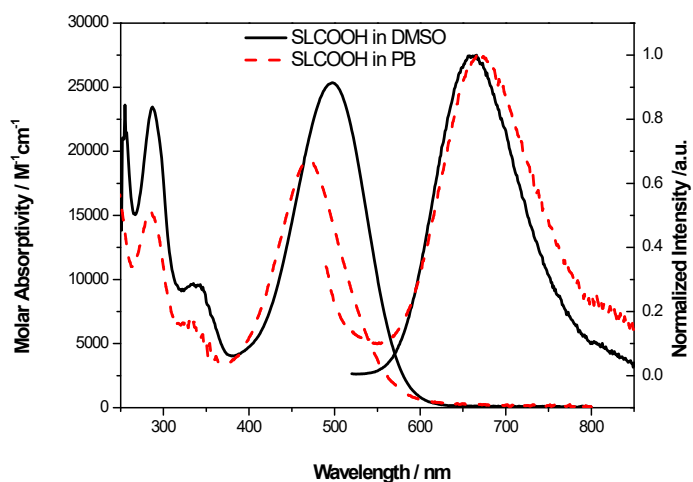


Fig. S1A. UV-vis absorption and emission spectra of **SLCOOH**.

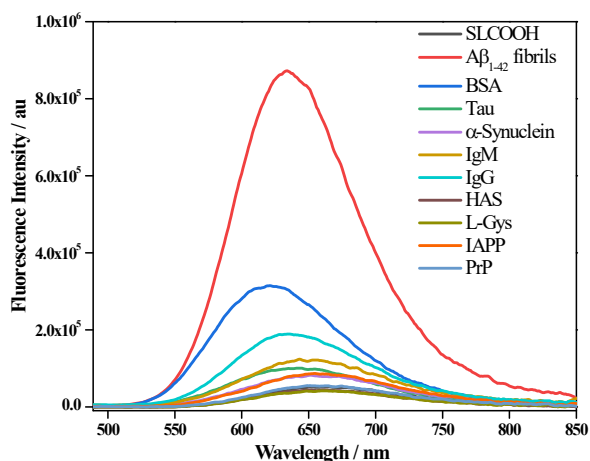


Fig. S1B. Fluorescence spectra of **SLCOOH** (10 μM) in the presence of 10 μM of $A\beta_{1-42}$ fibril, Tau-441 aggregate, BSA, α -Synuclein, IgM, IgG, HAS (Human Serum Albumin), L-Gys (L-Cysteine), IAPP (islet amyloid polypeptide) and PrP (prion protein) in 25 mM phosphate buffer (pH = 7.4).

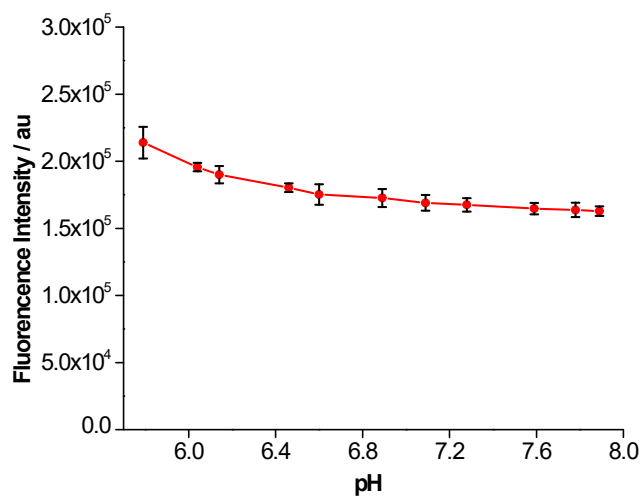


Fig. S1C. The pH effect on the fluorescence intensity of **SLCOOH** (30 μM) in 0.2 M phosphate buffer. Data are expressed as the mean \pm SD of three independent measurements ($n = 3$).

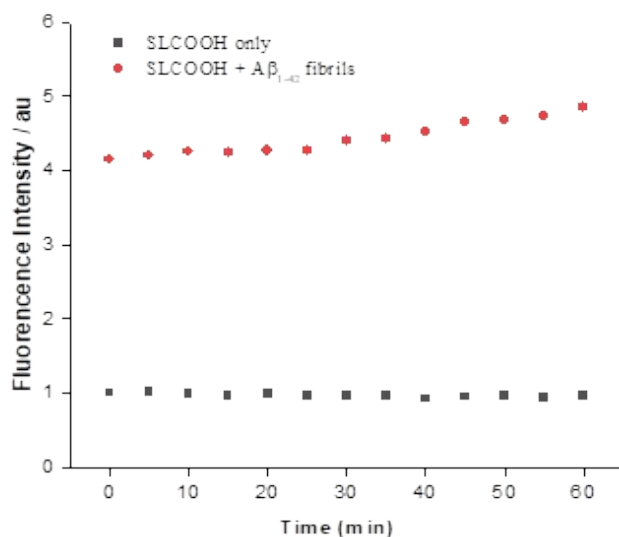


Fig. S1D. The time courses of fluorescence intensity of **SLCOOH** (30 μM) in the presence and absence of **A β_{1-42}** fibrils (150 μM).

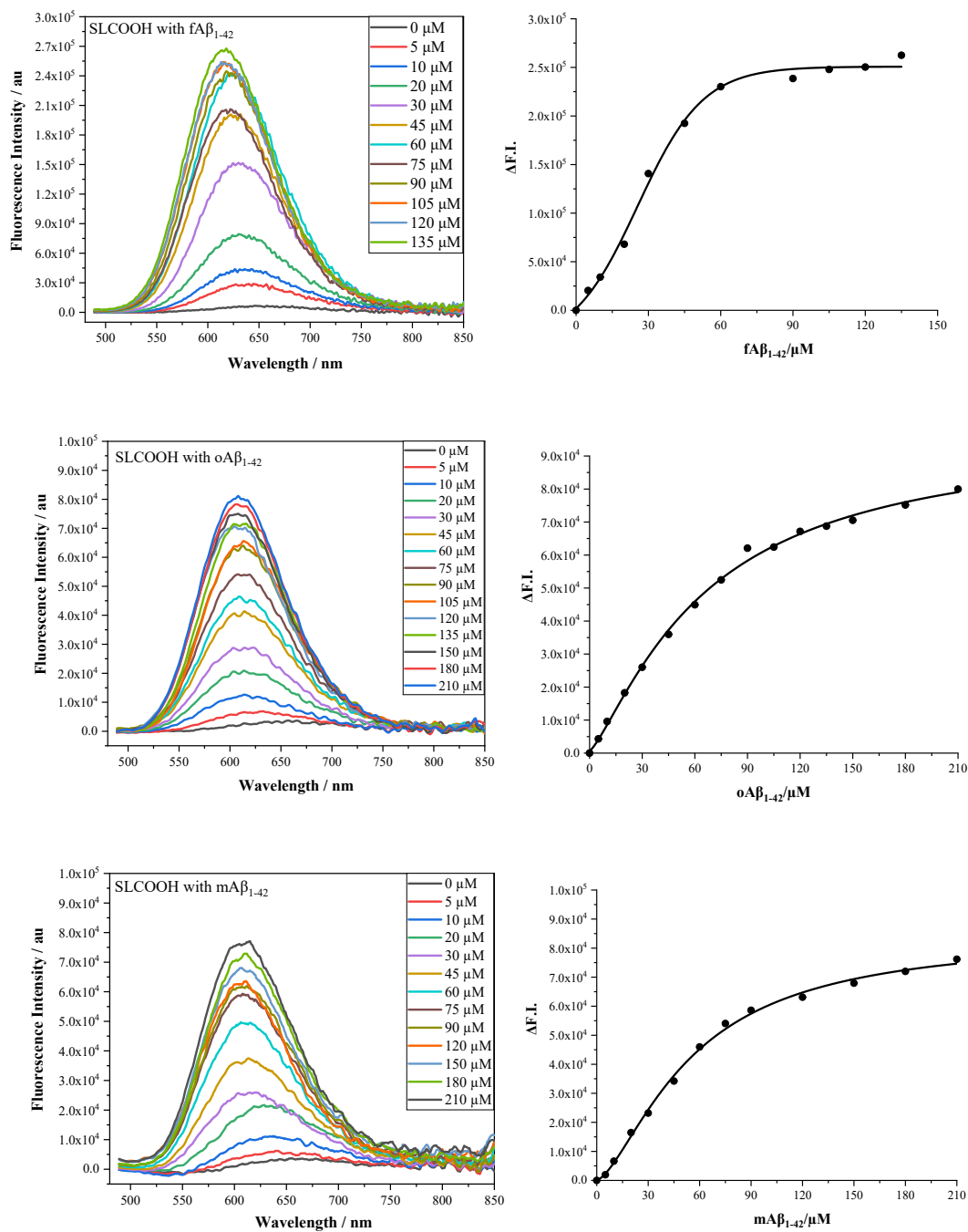


Fig. S1E. Fluorescence titration of A β ₁₋₄₂ species with SLCOOH and the respective saturation binding curves of SLCOOH to A β ₁₋₄₂ species, respectively.

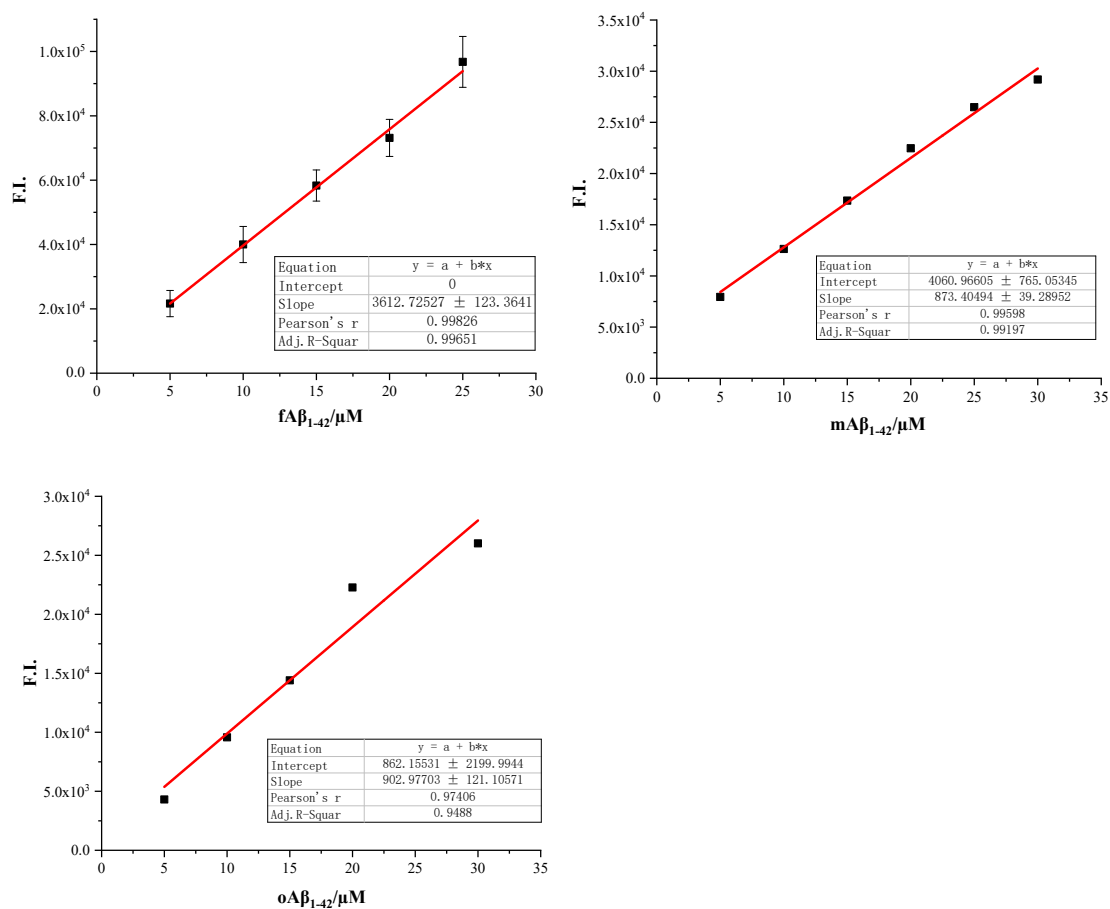


Fig. S1F. Plots of fluorescence change of SLCOOH (5 μM) in the presence of various concentrations of Aβ₁₋₄₂ fibril, Aβ₁₋₄₂ oligomer and Aβ₁₋₄₂ monomer in 25 mM phosphate buffer (pH = 7.4). The limit of detection was calculated by $3\sigma/k$ to be 0.52, 1.56, and 1.61 μM, respectively; where σ is the standard deviation of blank measurement; k is the slope.

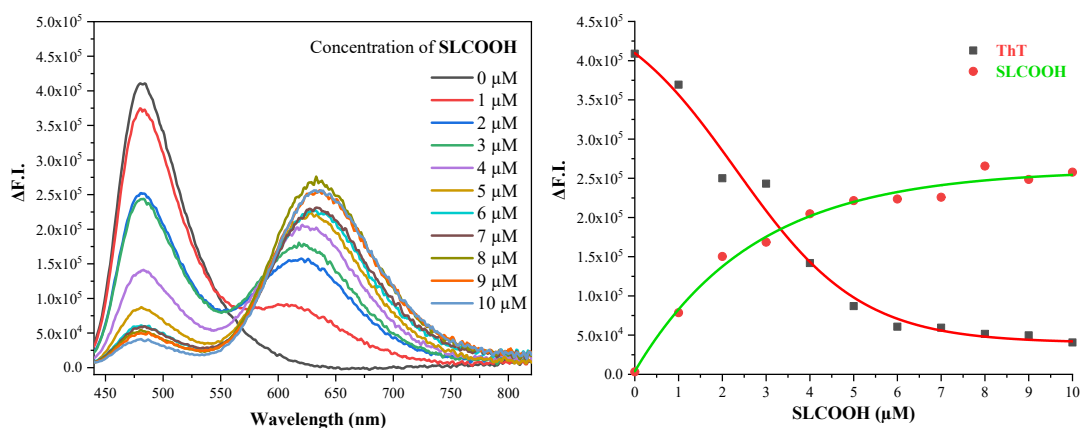
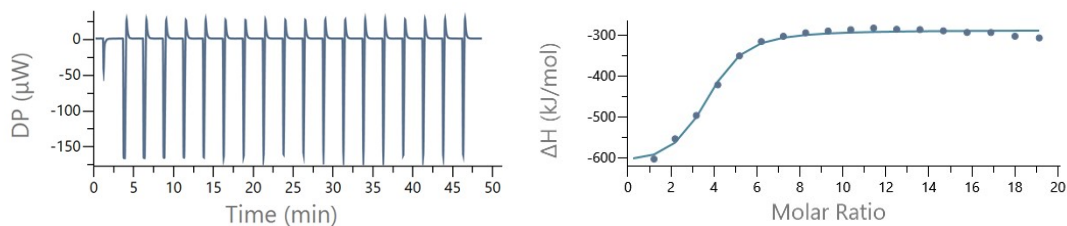
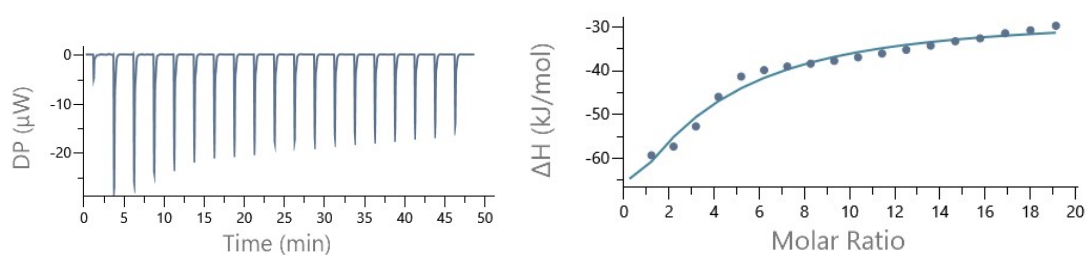


Fig. S1G. (a) Fluorescence spectra of ThT / $A\beta_{1-42}$ fibril complex (ThT, 5 μM / $A\beta_{1-42}$ fibrils, 10 μM) by adding SLCOOH ($c = 0-10 \mu\text{M}$) stepwise into the complex in 25 mM phosphate buffer (pH = 7.4) obtained by an excitation at 420 nm. (b) The curve fitting of the nonlinear plots of fluorescence intensity difference of ThT at 482 nm (green trace) and SLCOOH at 630 nm (red trace), respectively as a function of SLCOOH concentration.

(A)



(B)



(C)

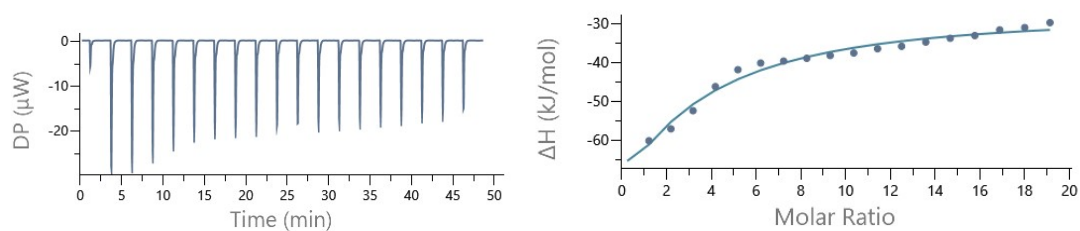


Fig. S1H. Isothermal titration calorimetry (ITC) binding profiles of SLCOOH and $A\beta_{1-42}$. (A) For $A\beta_{1-42}$ fibril: ICT thermogram and the binding isotherm from the integrated thermogram fit using the one-site model in the MicroCal PEAQ-ITC Analysis Software with $n = 3.40 \pm 0.099$, and $K_d = 4.54 \pm 1.09 \mu\text{M}$. (B) For $A\beta_{1-42}$ oligomers: ICT thermogram and the binding isotherm from the integrated thermogram fit with $n = 1.98 \pm 3.54$, and $K_d = 124 \pm 130 \mu\text{M}$. (C) For $A\beta_{1-42}$ monomer: ICT thermogram and the binding isotherm from the integrated thermogram fit with $n = 1.01 \pm 5.41$, and $K_d = 158 \pm 189 \mu\text{M}$.

Table S1. Summaries of optical properties of SLCOOH in different solvents

	Solvent	$\lambda_{\text{max}}^{\text{abs}} / \text{nm}$ ($\epsilon_{\text{max}} \times 10^4 / \text{M}^{-1}\text{cm}^{-1}$)	$\lambda_{\text{max}}^{\text{em}}{}^{\text{a}}$ (Stokes Shift) / nm	$\Phi_{\text{PL}}{}^{\text{b}}$
SLCOOH	DMSO	498 (2.53)	666 (168)	0.30
	PB	469 (1.93)	666 (197)	0.003

Table S2. Dissociation constant ($K_d(F_T)$), fluorescence enhancement factor, and limit of detection (LOD) of SLCOOH with various $A\beta_{1-42}$ species, respectively estimated from the fluorescence titration of $A\beta_{1-42}$ species with SLCOOH. Dissociation constant determined by ICT ($K_d(ICT)$)

	$mA\beta_{1-42}$	$oA\beta_{1-42}$	$fA\beta_{1-42}$
$K_d(F_T)(\mu\text{M})$	54.7	65.5	25.6
LOD (μM)	1.61	1.52	0.52

K_d (μM)

158

124

4.5

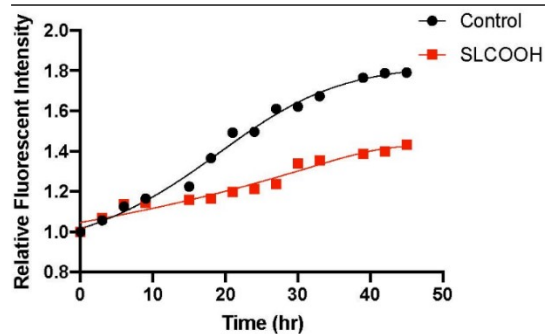


Fig. S2. Plots of the results of ThT fluorescence assay of $\text{A}\beta_{1-42}$ in the presence of SLCOOH.

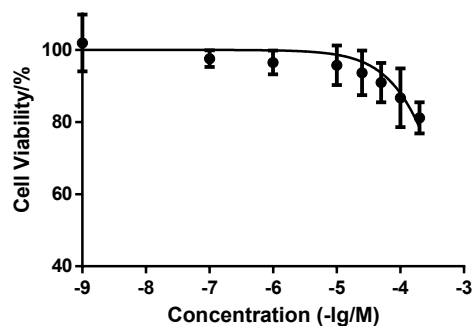


Fig. S3. Cell viability values (%) estimated by MTT proliferation. Human neuroblastoma SH-SY5Y neuronal cells were treated with different concentrations of SLCOOH at 37 °C for 24 h.

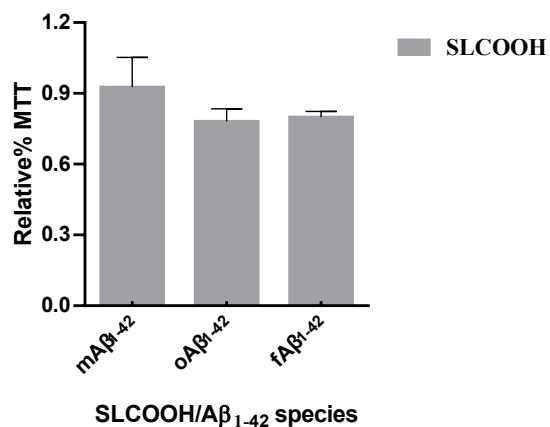


Fig. S4. Neuroprotective effect of SLCOOH against A β_{1-42} species toward SH-SY5Y neuronal cells.

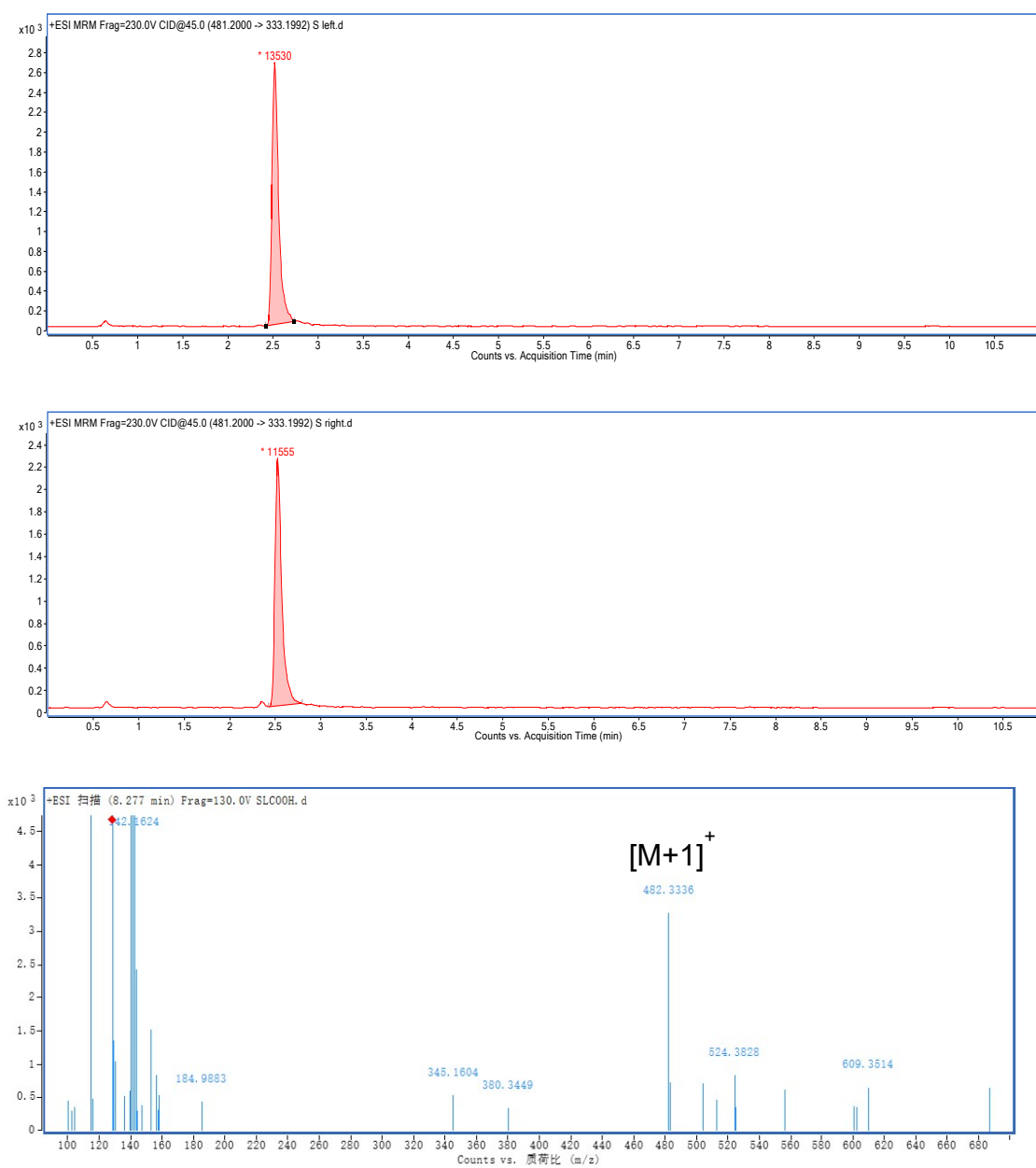


Fig. S5. LC-ESI-MS spectra of brain extracts of the SLCOOH-treated mice.

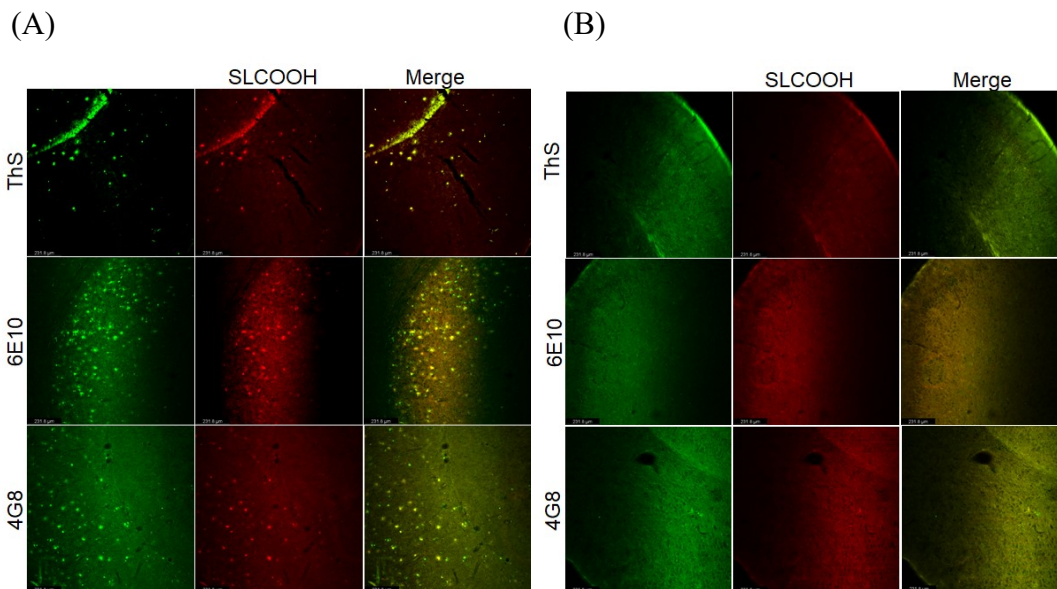


Fig. S6. *Ex vivo* images of SLCOOH in brain slices of (A) 6-month-old 5XFAD Tg and (B) age-matched WT mice co-localized with ThS and a primary antibody (6E10 and 4G8) and then a secondary antibody conjugated with Alexa 488.

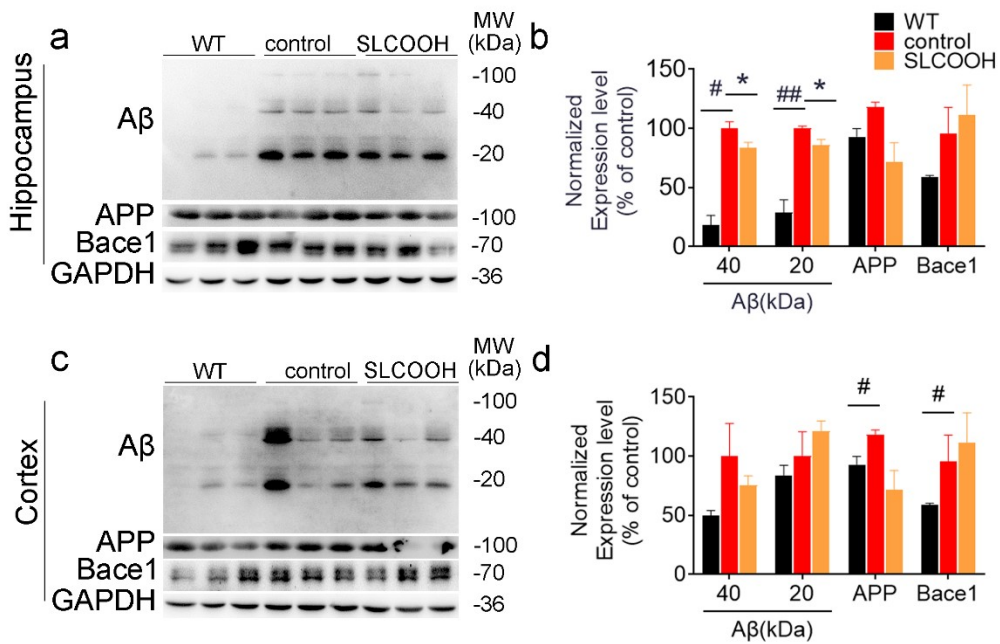


Fig. S7. SLCOOH treatment reduces A β levels in the hippocampus of AD mice. (a) Western blot analysis of A β , APP, and BACE1 protein levels in the hippocampus. (b) Densitometric analysis of (a). (c) Western blot analysis of A β , APP, and BACE1 protein levels in the cortex. (d) Densitometric analysis of (c) ($\#p < 0.05$, $\#\#p < 0.01$, $*p < 0.05$, $n = 6$).

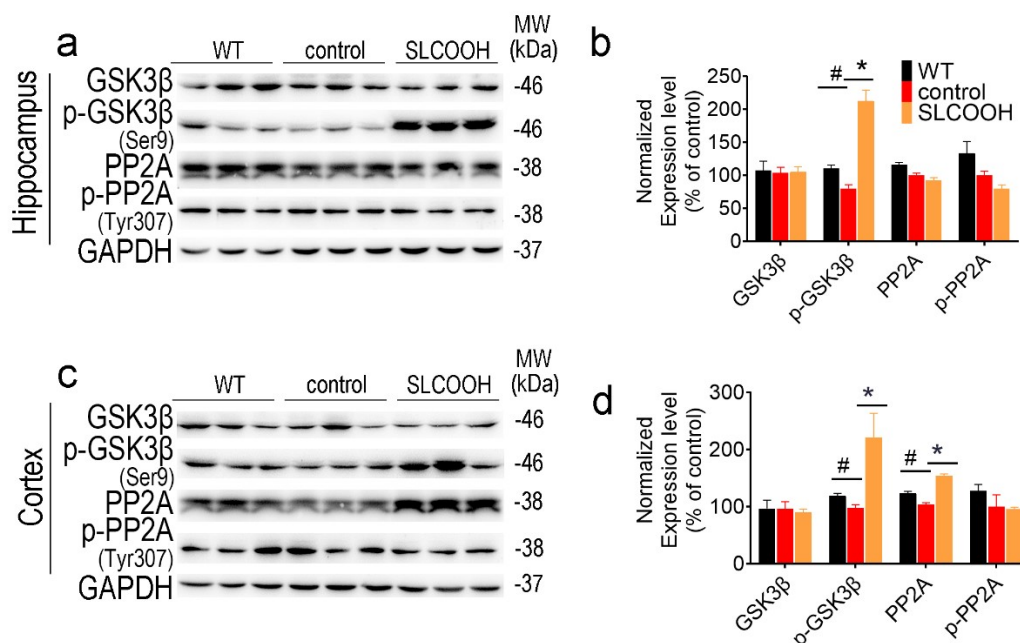


Fig. S8. SLCOOH reduces tau hyperphosphorylation by inhibiting the activity of GSK3 β but not PP2A in vivo. (a, b) Representative Western blot images (a) and quantification (b) of GSK3, p-GSK3 β (Ser9), PP2A, p-PP2A (Tyr307), expression levels in the hippocampus of WT, control and SLCOOH-treated mice. (c, d) Representative Western blot images (c) and (d) of the expression levels of these kinases in the cortex ($\#p < 0.05$, $*p < 0.05$, $n = 6$).

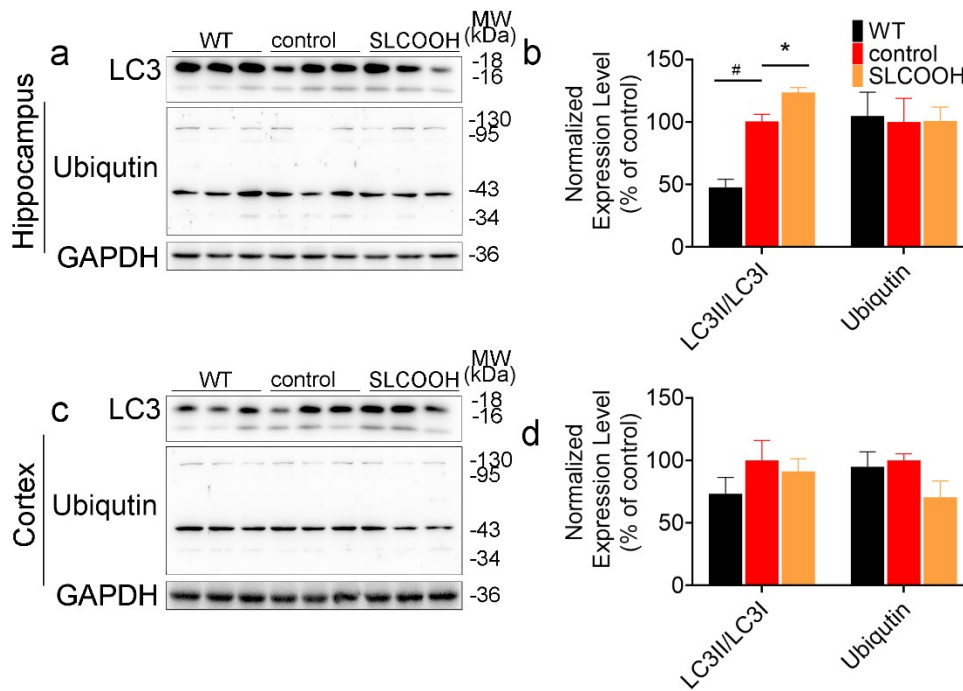


Fig. S9. SLCOOH promotes the formation of autophagosomes but not ubiquitin proteasomal system. (a, b) Representative Western blot images (a) and quantification (b) of LC3II/LC3I and ubiquitin protein expression levels in the hippocampus of WT, control and SLCOOH-treated mice. (c, d) Representative Western blot images (c) and quantification (d) of the expression levels of these kinases in the cortex (# $p < 0.05$, * $p < 0.05$, 1, $n = 6$).

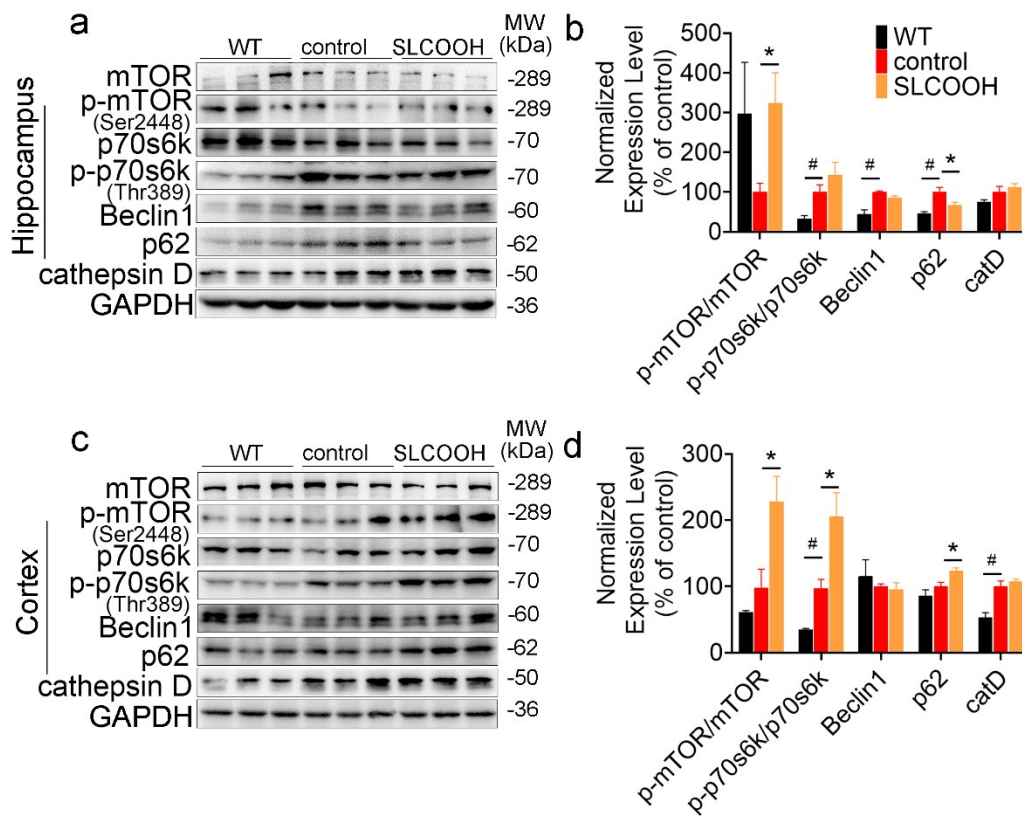


Fig. S10. SLCOOH increases initiation of autophagy pathway in vivo. (a, b) Representative Western blot images (a) and quantification (b) of mTOR/P-mTOR, and p70S6K/P-p70S6K, Beclin 1, p62, cathepsin D expression levels in the hippocampus of WT, control mice and SLCOOH-treated. GAPDH was used as the loading control. (c, d) Representative Western blot images (c) and quantification (d) of the expression levels of these kinases in the cortex. GAPDH was used as the loading control. (# $p < 0.05$, * $p < 0.05$, 1, n = 6).

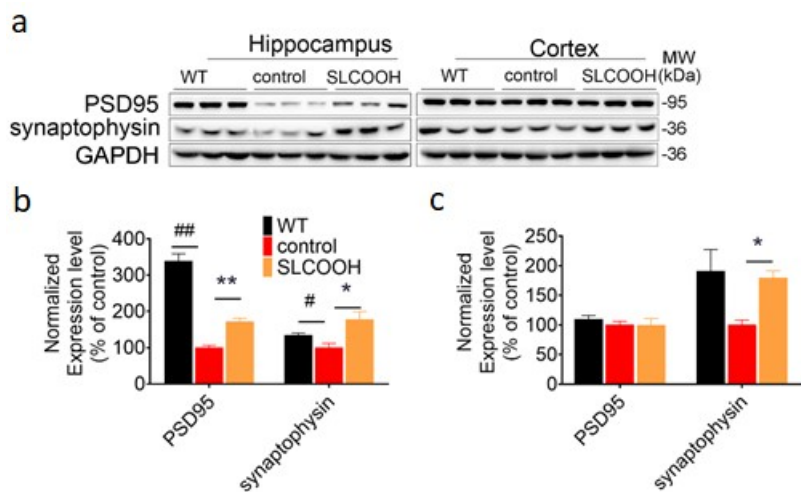


Fig. S11. (a) Representative western blots of PSD95 and Synaptophysin in the hippocampus and cortex. GAPDH was used as the loading control. (b and c) Densitometric analyses of the data in (a). (b) Hippocampus. (c) Cortex. ($##p < 0.01$, $*p < 0.05$, $**p < 0.01$, $n = 6$).

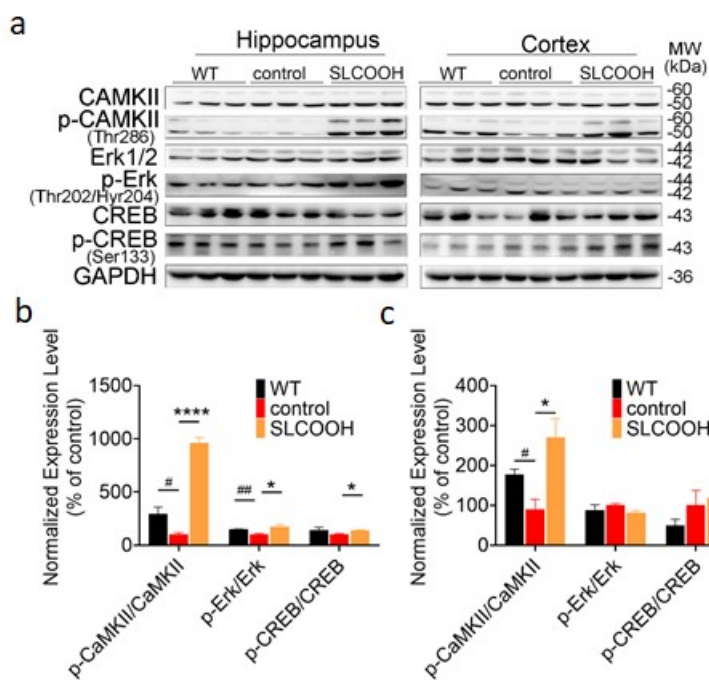


Fig. S12. (a) Representative western blots of CaMKII, p-CaMKII, ERK, p-ERK, CREB and p-CREB in the hippocampus and cortex of WT, AD and SLCOOH-treated mice at 6 months. GAPDH was used as the loading control. (b-c)

Densitometric analyses of the data in (a) (means \pm SEMs). (b) Hippocampus. (c) Cortex. ($\#p < 0.05$, $\#\# p < 0.01$, $*p < 0.05$, $****p < 0.0001$. $n = 6$)

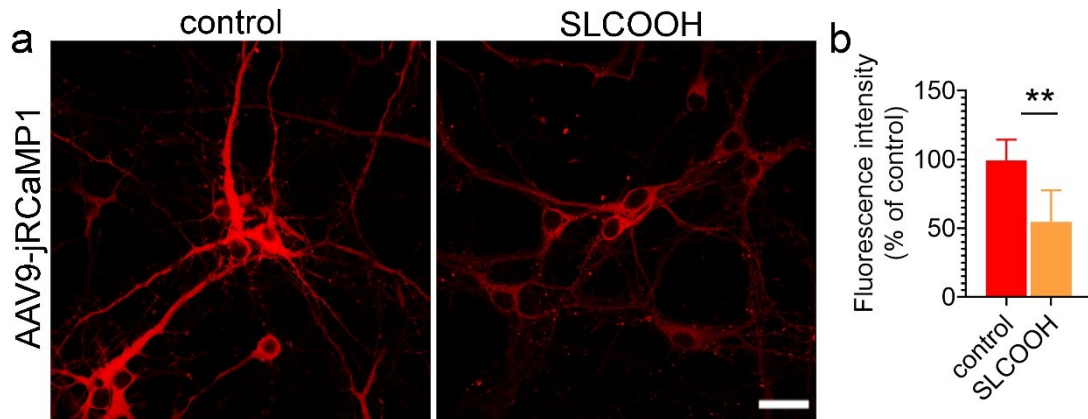


Fig. S13. SLCOOH alleviated the overload of intracellular Ca²⁺ in 3×Tg AD mice primary neurons. (a) Representative confocal images of intracellular Ca²⁺ in primary AD neurons transfected with AAV9-jRCaMP1. (Scale bar: 20 μ m) (b) The quantification of intracellular Ca²⁺ level. (** $p < 0.01$, $n = 6$ cells; The data was quantified from three independent experiments)

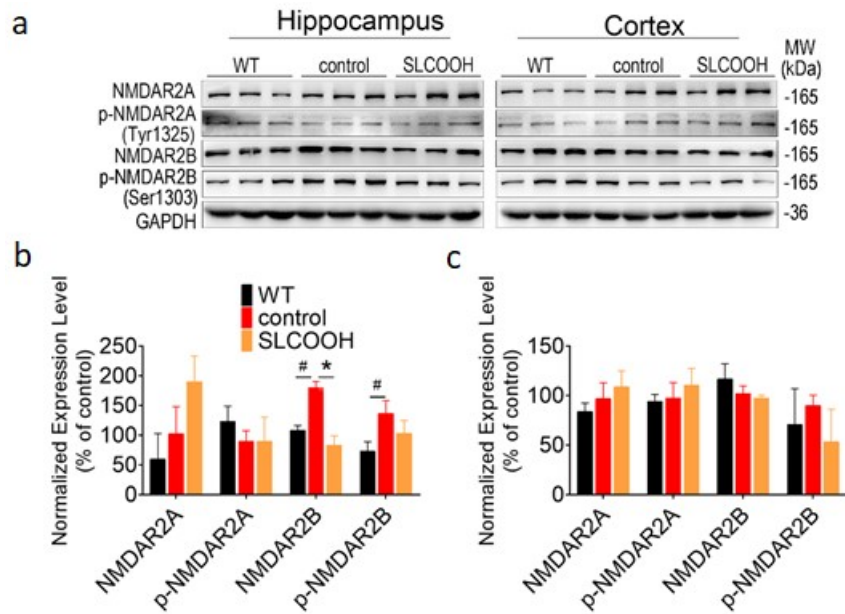
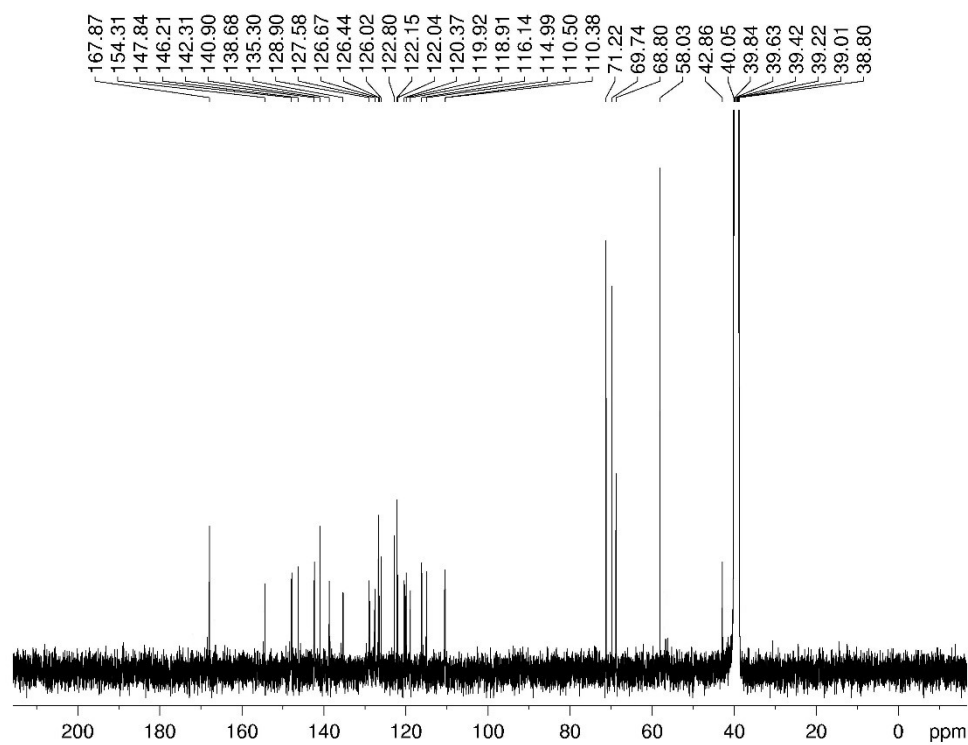
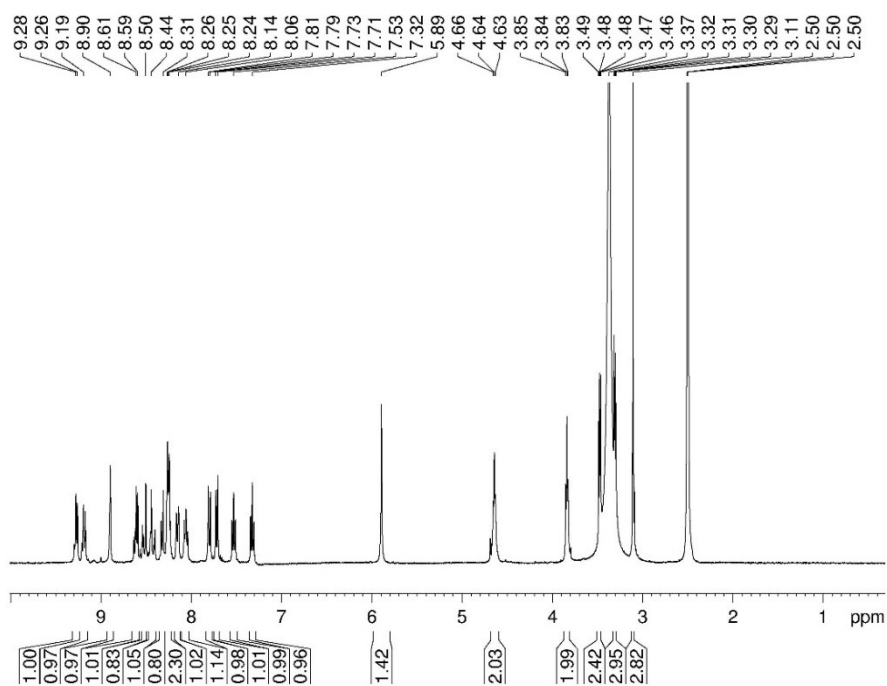


Fig. S14. SLCOOH decreases the intracellular Ca^{2+} level through downregulating the expression level of NMDAR2B. (a) Representative western blots of NMDAR2A, p-NMDAR2A, NMDAR2B, p-NMDAR2A in the hippocampus and cortex of WT, AD and SLCOOH-treated mice at 6 months. GAPDH was used as the loading control. (b-c) Densitometric analyses of the data in hippocampus (b) and cortex (c). (# $p < 0.05$, * $p < 0.05$, $n = 6$).



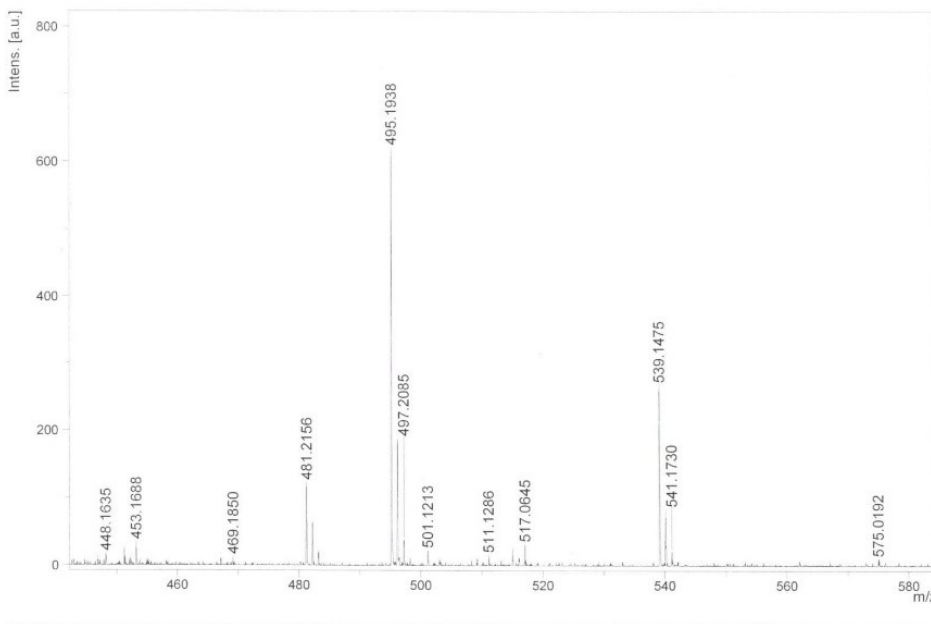
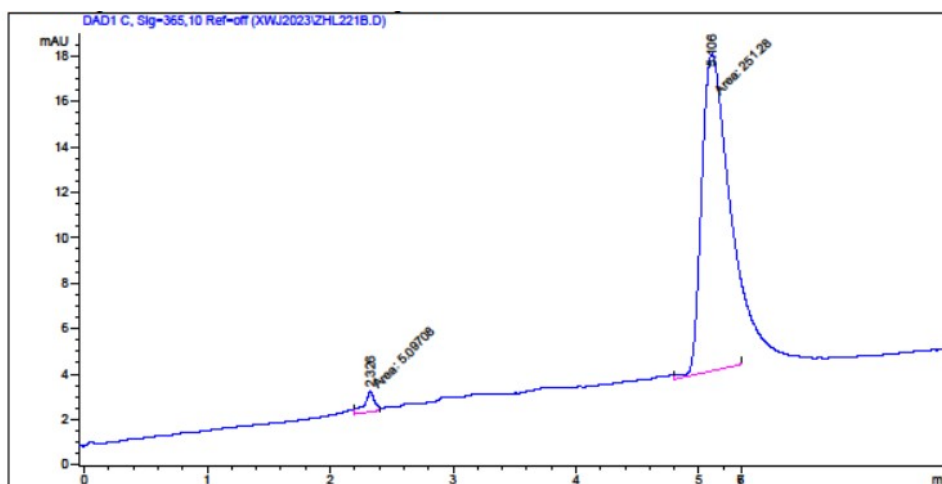


Fig. S15. ¹H and ¹³C NMR and HRMS spectra of SLCOOH.



=====
Area Percent Report
=====

Sorted By : Signal
Multiplier : 1.0000
Dilution : 1.0000
Sample Amount : 1.00000 [ng/ul] (not used in calc.)
Use Multiplier & Dilution Factor with ISTDs

Signal 1: DAD1 C, Sig=365,10 Ref=off

Peak #	RetTime [min]	Type	Width [min]	Area [mAU*s]	Height [mAU]	Area %
1	2.326	MM	0.0923	5.09708	9.20311e-1	1.9881
2	5.106	MM	0.2960	251.28032	14.14831	98.0119
Totals :				256.37740	15.06862	

Results obtained with enhanced integrator!
=====

Fig. S16. A HPLC trace of synthesized SLCOOH.